Evaluating Multi-seasonal SAR and Optical Imagery for Above-Ground Biomass Estimation Using the National Forest Inventory of Zambia

Kennedy Kanja[1,3,4], Ce Zhang[2], Peter M. Atkinson[1,5,6]

[1] Lancaster Environment Centre, Faculty of Science and Technology, Lancaster University, Lancaster LA1 4YG, UK

[2] School of Geographical Sciences, University of Bristol, Bristol BS8 1SS, UK

[3] School of Natural Resources, Copperbelt University, Kitwe, Zambia

[4] School of Applied Sciences, Kapasa Makasa University, Chinsali, Zambia

[5] Geography and Environmental Science, University of Southampton, Highfield, Southampton SO17 1BJ, UK

[6] College of Surveying and Geo-Informatics, Tongji University, No.1239, Siping Road, Shanghai, PR China, 200092

Abstract

Mapping forest above-ground biomass (AGB) is crucial for monitoring forest ecosystems and assessing the success of conservation initiatives such as the REDD+ carbon projects. Traditional field-based approaches to measuring AGB, however, face significant challenges, due to high financial costs and logistical constraints. Remote sensing, including both active and passive sensors, presents a promising and cost-effective alternative, yet its practical utility and accuracy for capturing forest AGB in diverse and complex ecosystems remains largely unexplored. This research used an extensive national forest inventory (NFI) dataset to evaluate the ability to map the AGB of the Miombo woodlands in Zambia across four agro-ecological zones using both multi-seasonal SAR (Sentinel-1A) and optical (Landsat-8 OLI) imagery. A multi-level experiment was designed to (i) compare the accuracy of AGB estimation using SAR and optical data when used independently, and in combination, using a Random Forest regression model, (ii) assess the effect of seasonality on the accuracy of AGB estimation when using SAR and optical datasets, and (iii) evaluate the effect of variation in climatic and environmental conditions on AGB estimation. Experimental results show that multi-seasonal images (across the rainy, hot and dry seasons) outperformed single-season and annual images. Combining SAR backscatter in the hot season, optical bands in the dry season, and vegetation indices in the hot season produced the most accurate AGB model ($R = 0.69$, MAE = 14.01 Mg ha^{-1} and RMSE = 18.23 Mg ha^{-1}). The models performed distinctly across different agro-ecological zones ($R = 0.44 - 0.79$), suggesting that fitting local models could be beneficial. These results based on the extensive NFI of Zambia demonstrate that seasonal effects and fitting local models can lead to more accurate AGB estimation within the Miombo woodlands, which is of significance for ongoing REDD+ carbon projects in Zambia and other African countries.

Keywords: Miombo woodlands; Above ground biomass; National Forest Inventory; SAR-optical; Remote Sensing, Random Forest

1. Introduction

Forest above-ground biomass (AGB) is an indispensable variable for forest monitoring, estimation of greenhouse gas emissions and sustainable management of carbon stocks, particularly for the REDD+ carbon projects (Saatchi et al., 2011; Harris, 2012; Wulder et al., 2012). High-quality forest AGB information, however, can be challenging to capture in tropical developing countries, due to financial costs and logistical constraints (Halperin et al., 2016a). In particular, traditional field-based approaches that are used commonly in developing countries demand huge time and labour, and may be impractical due to inaccessibility when conducting regional-to-national scale forest AGB estimation (Atkinson et al., 2000; Ghosh and Behera, 2018). Remote sensing-based methods, by combining field observed AGB and remote sensing datasets, can overcome many of these limitations, although they present additional challenges, dependent upon the satellite sensors and platforms (Carreiras et al., 2012; Lu et al., 2016). Active and passive sensors can both be used to map forest AGB, but active sensors such as light detection and ranging (LiDAR) and synthetic aperture radar (SAR) can be more effective for forest AGB estimation compared to passive sensors, thanks to their ability to interact with vegetation structures (Herold et al., 2019; Li et al., 2020). Challenges associated with SAR involve susceptibility to water content, terrain variation and the spatial arrangement of forests (Chen et al., 2023). Forest AGB is highly correlated with optical data, but optical data are limited by weather conditions, and vegetation indices produced from optical data commonly saturate at high biomass and dense canopy cover (Halperin et al., 2016b; Joshi et al., 2016; Zhao et al., 2016; Gascón et al., 2019).

Tremendous efforts have been made in mapping forest AGB in tropical forests using both active and passive sensors (Cassells et al., 2009; Carreiras et al., 2012; Gizachew et al., 2016; Ghosh and Behera, 2018; Gou et al., 2019; Van Pham et al., 2019; Zimbres et al., 2021; David et al., 2022b). However, most studies focused on tropical rainforests, such as the Brazilian Amazon (Kuplich et al., 2005; Salis et al., 2006; Quijas et al., 2019; Zimbres et al., 2021). L-band SAR data have been used frequently for forest AGB estimation with high accuracy, with their ability to penetrate tree crowns (Carreiras et al., 2012; Mitchard et al., 2013b; McNicol et al., 2018b; Gou et al., 2019). ALOS PALSAR L-band data, for example, were adopted to map forest AGB in Southern Africa and produced the first continental forest AGB map of the African savannahs and woodlands (Urbazaev et al., 2015; Bouvet et al., 2018). LiDAR, which has the ability to estimate canopy height and structure, shows potential for retrieval of forest biophysical parameters, such as volume and biomass (Pirotti, 2011; Kanja et al., 2019a; Pearse et al., 2019; Demol et al., 2024; Li et al., 2024). Nevertheless, the majority of SAR and LiDAR data are not freely available and impractical at regional and national scales. Sentinel-1 SAR C-band data from the European Space Agency, on the other hand, are offered free of charge. The combination of field observed AGB, SAR and optical satellite sensor imagery can be useful to estimate forest AGB in regions where data are scarce, such as in developing countries (Forkuor et al., 2020; Li et al., 2020).

The Miombo woodlands, found across South and East Africa, are characterised by a closed canopy that is not too dense, thereby allowing the growth of a herbaceous layer (Campbell, 1996). They extend over Angola, Malawi, Zimbabwe, Mozambique, Zambia, Tanzania, and part of Congo DRC, making them the most widespread woodland type in Africa. Miombo woodlands are an important source of livelihoods for people living in these countries, as they provide multiple ecosystem functions and services (Syampungani et al., 2009; Chidumayo and Gumbo, 2010; Kalaba et al., 2013; Ryan et al., 2016). Despite progress in combining SAR and optical data for forest mapping, most previous studies mapped Miombo woodlands using optical data alone (Gizachew et al., 2016; Halperin et al., 2016a; Mayes et al., 2016; Mareya et al., 2018), whereas some studies tested SAR data and LiDAR data separately (Cassells et al., 2009; Mitchard et al., 2013a; McNicol et al., 2018a; Gou et al., 2019; Demol et al., 2024; Li et al., 2024). Few studies used a combination of SAR/LiDAR and optical data to increase the accuracy of Miombo woodland AGB mapping (Næsset et al., 2016; Egberth et al., 2017; David et al., 2022a; Macave et al., 2022). For example, David et al. (2022) used Sentinel-1 and Sentinel-2 data for forest AGB estimation in the tropical dry forests of Botswana, while Macave et al. (2022) utilized Landsat-8, Sentinel-2A, Sentinel-1B and ALOS/PALSAR-2 to estimate forest AGB in the Miombo woodlands of Mozambique. Both studies led to an increased accuracy, although their coverage was limited to National Parks only. To the best of our knowledge, no studies used national forest inventory (NFI) data to validate models that combine SAR and optical data to estimate forest AGB in the Miombo woodlands at regional-to-national scales. Gascón et al. (2019) explored the potential to estimate forest AGB at the national level in Tanzania using national survey data but using optical data (RapidEye) alone (Gascón et al., 2019). Moreover, very few studies explored the seasonal effects of SAR and optical data on forest AGB mapping (Laurin et al., 2018; Forkuor et al., 2020; Chen et al., 2023; Tanase et al., 2024), which could be important for the Miombo woodlands as a tropical dry forest. The use of multi-seasonal data is aimed at taking advantage of the relation between AGB and images under varying phenological conditions (Zhu and Liu, 2015; Chrysafis et al., 2019). Studies that compared the use of single images and multi-seasonal images for AGB estimation concluded that multi-seasonal images predicted more accurately than single images (Zhu and Liu, 2015; Cartus and Santoro, 2019; Chen et al., 2023). However, none of these studies explored fully the phenological conditions that vary with the seasons by compositing the mean seasonal images.

To address these gaps, this research aims to test and evaluate multi-seasonal Sentinel-1A and Landsat-8 OLI imagery to estimate forest AGB in Zambia's Miombo woodlands across four agro-ecological zones, using an extensive NFI ground reference dataset available from the Forestry Department of Zambia that has not been used for this purpose before. Specific objectives include (1) to evaluate model prediction accuracy when SAR and optical data are used independently and when they are combined, (2) to determine the optimal time period (annual, rainy, dry, hot, multi-season) for forest AGB estimation in the Miombo woodlands when using SAR and optical data, (3) to analyse and compare model uncertainties across four agro-ecological zones characterised by different climatic conditions, terrain conditions and vegetation types, and (4) to predict wall-to-wall forest AGB using the best fitting relationship between NFI and SAR and optical data. This research adds to the improvement of forest AGB estimation by combining multi-seasonal SAR and optical remote sensing data with an NFI dataset, providing a novel approach to biomass mapping in tropical dry forests like Zambia's Miombo woodlands. The outcomes of this research enhance the accuracy of large-scale AGB assessments, and thereby making available the much-needed AGB maps for evidence-based forest management, REDD+ carbon projects, and policy formulation.

2. Methodology

2.1 Study Area

This research was conducted in Zambia (Fig. 1), with its forest landscape being considered for REDD+ projects presently (Handavu et al., 2021). Our primary focus is on the dominant Miombo woodlands, and Miombo woodlands mixed with Mopane, Hill and Karahali woodlands. Both dry and wet Miombo woodlands are represented extensively in Zambia. Dry Miombo woodlands are characterised by trees with heights less than 15 m and few canopy overlaps, and receive annual rainfall of less than 1000 mm, represented by agro-ecological zones I, IIa and IIb (Fig. 1). Agro-ecological zone I is characterised by hot and dry areas, receives lower annual rainfall of 800 mm and below, and has lower altitudes of 400-900 m. Agro-ecological zone IIa forms part of an area that receives medium annual rainfall of 800-1000 m with an altitude between 900 and 1300 m. Agro-ecological zone IIb completes the area that receives medium rainfall comprising of sand and floodplains with an altitude between 900 and 1300 m. Wet Miombo woodlands are characterised by trees of more than 15 m height with crown overlap in some cases where the annual rainfall received is more than 1000 mm. Wet Miombo is associated with agro-ecological zone III which receives high rainfall with altitudes between 1100 and 1500 m (Chidumayo and Gumbo, 2010; Bulusu et al., 2021; Shamaoma et al., 2022). These zones cover all available environments in Zambia with dry woodlands extending into neighbouring countries in the south and east, and wet woodlands extending into countries in the north and east of Zambia.

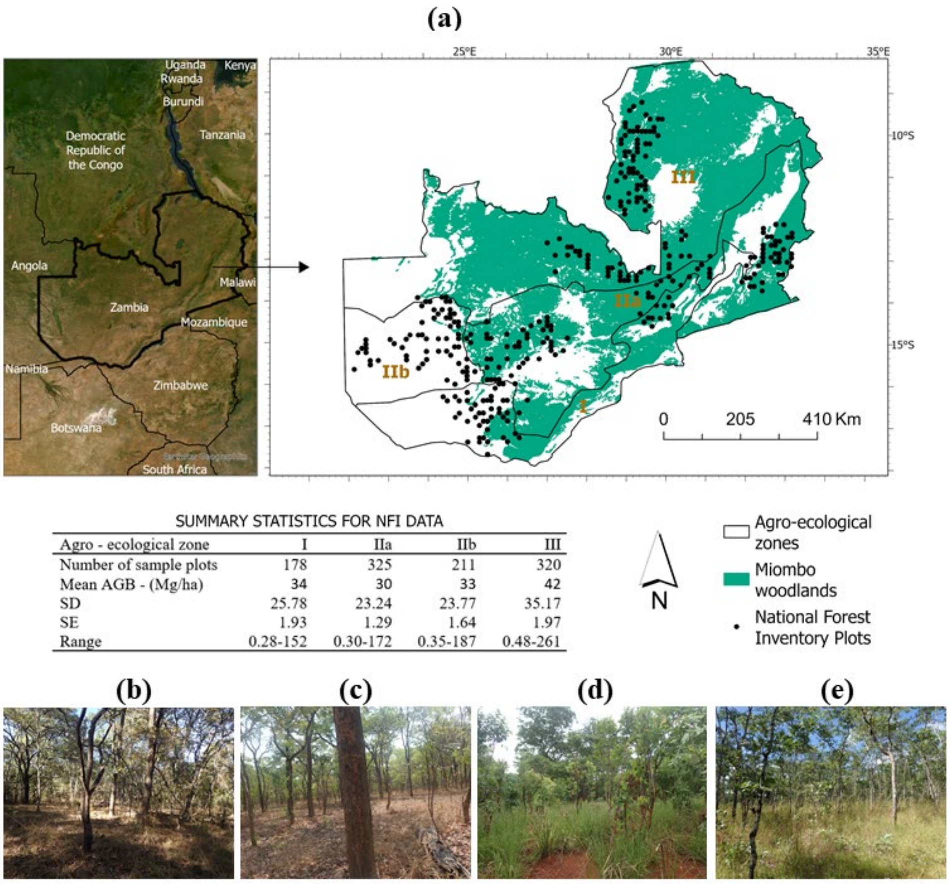

Agro - ecological zone	I	IIa	IIb	III
Number of sample plots	178	325	211	320
Mean AGB - (Mg/ha)	34	30	33	42
SD	25.78	23.24	23.77	35.17
SE	1.93	1.29	1.64	1.97
Range	0.28-152	0.30-172	0.35-187	0.48-261

Fig. 1. Study area map and typical ground photos showing Miombo woodlands. (a) The location of the National Forest Inventory plots used in this research, spread across Zambia's

four agro-ecological zones I, IIa, IIb and III, together with some summary statistics. (b) and (c) primary Miombo woodlands, (d) and (e) disturbed Miombo woodlands.

2.2 Data acquisition

2.2.1 National Forest Inventory data

The NFI data used in this research were collected for the Integrated Land-Use Assessment Phase Two project (ILUA-II), which took place between 2010 to 2016. The ILUA-II was the largest forest inventory of Zambia, undertaken by the Forestry Department, with technical assistance from the Food and Agriculture Organisation of the United Nations (FAO) and funded by the Government of Finland (Shakacite et al., 2016.).

The NFI plots were distributed across all major vegetation types in Zambia and stratified with forest variation (Shakacite et al., 2016.). The four agro-ecological zones present a variety of vegetation types with each zone representing a different climatic condition that affects vegetation type and growth. A total of 1034 NFI plots were used for the current research covering all four agro-ecological zones (Fig. 1). 60% of these inventory plots covered Miombo woodlands, 14% Karahali woodlands, 10% Hill woodlands and 7% Mopane woodlands.

Four plots measuring 0.1 ha (20 m by 50 m) formed a cluster. Fig. 2 shows a schematic representation of the spatial arrangement of four plots within each cluster. The plots, and not the clusters, within which trees with Diameter at Breast Height (dbh) above 10 cm were recorded formed the basic sampling units of this research. Refer to Shakacite et al., (2016) for details. Only those forest inventory plots captured in 2014, and shown in Figure 1, were considered for this research to correspond as closely as possible to the availability of Sentinel-1 SAR data. However, 951 plots were ultimately used during the regression analysis due to non-availability of remote sensing data for certain time periods.

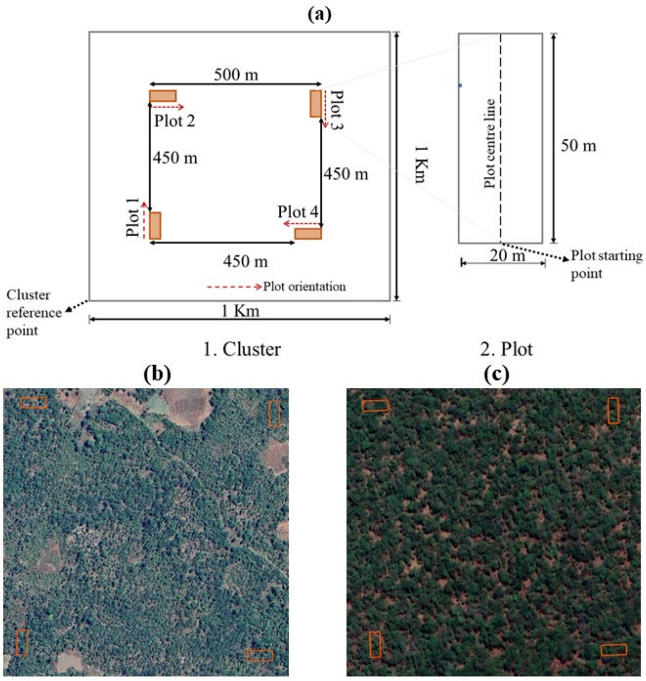

Fig. 2. Configuration of data collection sites. (a1) cluster design, (a2) plot design, (b) and (c) two random clusters showing field observed NFI plots (disturbed and intact, respectively) superimposed on Google Earth Imagery.

2.2.2 Remote sensing data

Sentinel-1 Ground Range Detected (GRD) scenes from ESA's Sentinel 1 satellites (A and B) in dual polarisation SAR C-band were downloaded from Google Earth Engine (GEE). We processed the Sentinel-1 (S1) data by filtering based on study area, time period, instrument mode (IW) and polarisation (VV, VH). Backscatter coefficients for the VH and VV polarizations, together with texture information, were retrieved and employed as SAR predictor variables (covariates) in the forest AGB regression analysis.

We used a similar approach for retrieving the optical spectral bands, texture information and vegetation indices from the Landsat-8 Operational Land Imager (OLI). We used Landsat 8 (L8) level 2, Collection 2 which contains atmospherically corrected surface reflectance images, with the cloud cover threshold set as 1%, representing close to cloud free. The Landsat-8 images were then resampled to 10 m pixel size to align with the Sentinel-1 data and to fit within the inventory plots. Five spectral vegetation indices were selected based on similar studies, including the normalised difference vegetation index (NDVI) (Gizachew et al., 2016), normalised difference moisture index (NDMI) (Halperin et al., 2016a), normalised difference water index (NDWI) (Jha et al., 2021), bare soil index (BSI) (Xie et al., 2022) and enhanced vegetation index (EVI) (Lembani et al., 2020).

The Grey Level Co-occurrence Matrix (GLCM) texture method in GEE was utilised to derive texture metrics with input grey-level images generated using eqs. 1 and 2 for S1 and L8, respectively, with window sizes of 2 and 5 pixels (Tassi et al., 2021; Vizzari, 2022).

We used Landsat-8 images from 2014, but Sentinel-1 images were limited in number and, thus, ended up using the 2015 images due to the non-availability of Sentinel-1 images in 2014.

$$\text{L8 Gray-level Image} = (0.3 * NIR) + (0.59 * RED) + (0.11 * GREEN) \quad (1)$$

$$\text{S1 Gray-level Image} = (VH - VV) / (VH + VV) \quad (2)$$

To assess seasonal effects and determine an optimal time period for forest AGB estimation using remote sensing SAR and optical data, we considered three distinct seasons: namely, the wet and rainy season (occurring from mid-November to April, hereafter referred to as rainy season), the cool and dry season (occurring from May to mid-August, hereafter referred to as dry season) and the hot and dry season (occurring from mid-August to mid-November, hereafter referred to as hot season) (Zambia - Climatology | Climate Change Knowledge Portal (worldbank.org)). The annual average was also created as a comparison. We applied a mean-based reduction filter for each time period.

2.3 Above ground biomass modelling

Fig. 3 presents an overview of the methodology. The steps taken from data collection to producing the forest AGB maps can be summarised as (1) Sentinel-1 and Landsat-8 data composition, (2) NFI data processing and (3) modelling and evaluation.

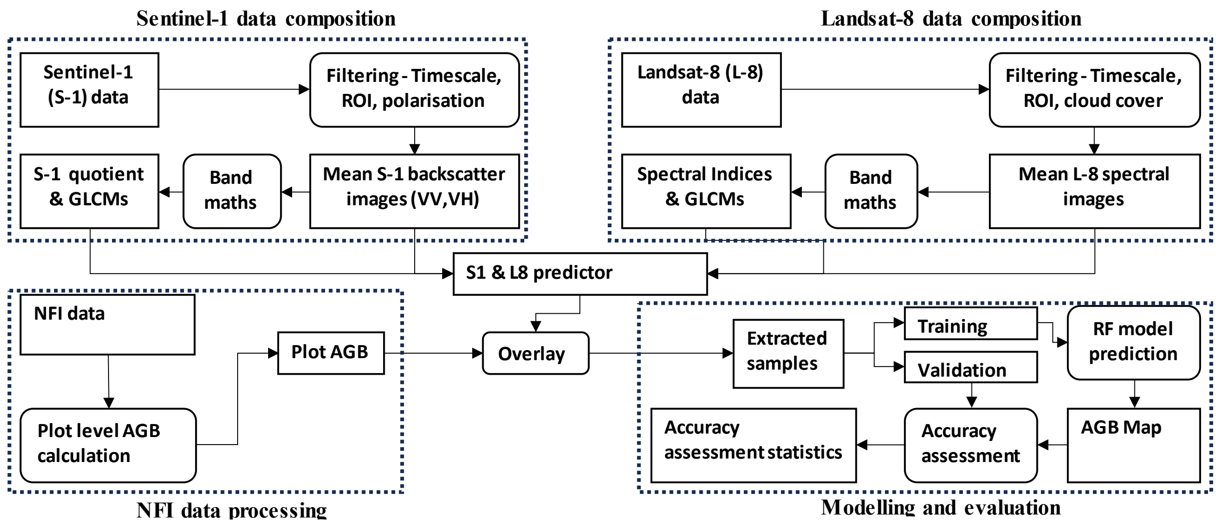

Fig. 3. Overview of methodological approach for forest above ground biomass modelling

2.3.1 Plot AGB calculation

We estimated plot AGB using tree inventory data collected during the ILUA-II project. All standing trees measured per plot in line with the ILUA II field protocol, described in Shakacite et al. (2016), were considered. We used both a locally calibrated allometric model developed by Chidumayo (eq. 3) and a generalised biomass estimation model for tropical forests recommended by Chave et al. (eq. 4), to calculate individual tree AGB and establish AGB for each plot by summation (Chidumayo, 2012.; Chidumayo, 2013; Chave et al., 2014). Plot AGBs for the two models were highly correlated (r=0.96). We noted that AGB calculated using

Chidumayo's allometric model was more consistent compared to Chave's model which might be attributed to the non-availability of some tree species' wood specific densities (ρ). The ILUA II project also adopted the Chidumayo model and, therefore, the plot AGBs were derived using Chidumayo's allometric model to allow effective comparison (Chidumayo, 2013; Shakacite et al., 2016.).

$$\mathrm{AGB_{tree}} = \exp(2.342 \ * \ln(\mathrm{dbh}) - 2.059) \quad (3)$$

$$\mathrm{AGB_{tree}} = 0.0673 \times (\rho D^2 H)^{0.976} \quad (4)$$

where dbh in eq. (3) and D in eq. (4) represent the diameter at breast height, ρ is the wood specific density and H is the absolute tree height.

Both plot AGB and remote sensing variables were extracted based on the basic sampling unit (0.1ha). Total plot AGB was converted to AGB per ha while the pixel average within the basic sampling unit was extracted for remote sensing variables.

2.3.2 Correlation between forest AGB and remote sensing covariates

Pearson correlation coefficients between forest AGB and the remote sensing covariates were calculated. We analysed these correlation coefficients for all four time periods and across the four agro-ecological zones. The results were used to conduct a preliminary selection of optimal remote sensing variables. Only those covariates with correlation coefficients equal to or above 0.2 ($r >= |0.2|$) were considered for the subsequent regression analysis (Fagua et al., 2019).

2.3.3 Remote sensing variable importance

Variable importance can be useful in selecting optimal variables from a high dimensional dataset (Li et al., 2020). Here, we made use of the variable importance feature in the random forest regression algorithm. This analysis assisted in refining the final variable selection for each model and provided future guidance for optimal remote sensing data acquisition (best time period and variables to consider) for forest AGB estimation in the Miombo woodlands.

2.3.4 Random forest regression modelling

Random forest (RF) regression models were used for forest AGB prediction (Breiman, 2001). RF models work by creating hundreds of decision trees in an ensemble, for making predictions. The relationship between forest AGB and remotely sensed variables is usually nonlinear, and non-parametric machine learning algorithms are used widely to increase accuracy above parametric models (e.g. linear regression), as they do not require a specific distribution (Ghosh and Behera, 2018; David et al., 2022a). The non-parametric RF algorithm was adopted to handle high-dimensional features and nonlinear relationships between forest AGB and remote sensing data, given its wide application for forest AGB estimation (Forkuor et al., 2020; Li et al., 2020; Chen et al., 2023). We varied the number of trees (maximum iteration) until optimal results (at 2000 trees) were achieved based on the validation R^2 and RMSE. In contrast, the maximum tree depth was data-driven, and the default was used for the number of randomly sampled variables.

2.3.5 Experimental design

We designed a multi-level experiment using NFI data to compare several forest AGB estimation models (Table 1):

(1) Using SAR data alone and using optical data alone, against models using combined SAR and optical data
(2) Using various seasonal datasets for each of the three cases (SAR, optical, and SAR+optical)
(3) Assessing the effect of varying climatic and environmental conditions across four agro-ecological zones on the accuracy of forest AGB estimation.

Table 1
Structure of the multi-level experiment to evaluate approaches for estimating forest AGB in Zambia's Miombo woodlands.

Sensor	Time period	Model	Abbreviation	Number of variables
SAR	Rainy	S1 rainy	S1-r	20
	Hot	S1 hot	S1-h	20
	Rainy and Hot	S1 rainy & hot	S1-r & h	40
	Annual	S1 annual	S1-y	20
Optical	Dry	L8 dry	L8-d	28
	Hot	L8 hot	L8-h	28
	Dry and Hot	L8 dry & hot	L8 d & h	56
	Annual	L8 annual	L8-y	28
SAR and optical	Hot	S1L8 hot	S1L8-hot	48
	Multi-season	S1L8 Multi-season	S1L8-m	96
	Annual	S1L8 annual	S1L8-y	48

Note, optical images were not available for the rainy season due to excessive cloud cover, and Sentinel-1 SAR images were not available for the dry season in 2015. Both were excluded from the subsequent analysis.

2.4 Accuracy assessment

We tested the prediction accuracy of each model using a validation dataset, comprising 15% of the available data that were not employed during the model training. This single set-aside validation dataset was maintained for effective comparability of the experiments. The multiple correlation coefficient (R, eq. 5), mean absolute error (MAE, eq. 6), root mean square error (RMSE, eq. 7), and the symmetric mean absolute percentage error (SMAPE) were used to assess model performance (Malhi et al., 2021). We added SMAPE to the three frequently used error statistics as it is a relative error and works well when comparing model prediction accuracies (Forkuor et al., 2020; Chen et al., 2023).

$$R = \left(1 - \frac{\sum_{i=1}^{n}(O_i - P_i)^2}{\sum_{i=1}^{n}(O_i - M)^2}\right)^{\frac{1}{2}} \qquad (5)$$

$$\text{MAE (Bias)} = \frac{1}{n}\sum_{i=1}^{n} \mid O_i - P_i \mid \quad (6)$$

$$\text{RMSE} = [n^{-1} \sum_{i=1}^{n}(P_i - O_i)^2]^{\frac{1}{2}} \quad (7)$$

$$\text{SMAPE} = \frac{1}{n} \sum_{i=1}^{n} \frac{\mid O_i - P_i \mid}{(\mid O_i \mid + \mid P_i \mid)/2} \quad (8)$$

where *n* is the number of sample plots, *O* is the field observed forest AGB, *P* is the predicted forest AGB, and *M* is the mean forest AGB calculated from the field observed forest AGB.

3 Results

3.1 Ground observed forest AGB and tree density

Fig. 4 (a) and (b) show the distribution of forest AGB and tree density, respectively, across the four agro-ecological zones. Agro-ecological zone III, wet Miombo, recorded the largest mean forest AGB and the highest mean tree density. The agro-ecological zones covering dry Miombo had lower mean forest AGBs and tree densities with minimal differences, compared to wet Miombo. Dry Miombo Agro-ecological zones I, IIa and IIb recorded small forest AGB standard deviations (SD), relative to agro-ecological zone III (Fig. 1 A).

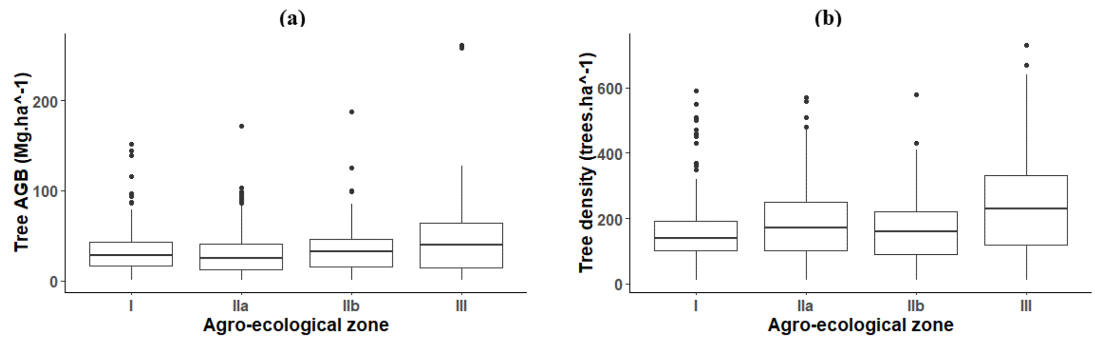

Fig. 4. Boxplots showing (a) plot AGB and (b) tree density across the four agro-ecological zones.

3.2 Correlation analysis between forest AGB and predictor variables

We computed the Pearson product-moment correlation coefficient between forest AGB and the predictor variables, Figs. S1-S9. For the SAR data, both raw polarisations (VV, VH) produced large correlation coefficients with forest AGB compared to the SAR texture bands. VH backscatter was correlated with forest AGB higher than VV backscatter. For optical data, the visible and shortwave infrared bands produced larger correlation coefficients compared to the near infrared band across all seasons. All the vegetation indices considered in this research produced correlations above the set threshold. Among the texture variables that produced larger correlations with forest AGB, the difference variance (dvar) was the largest.

Overall, the largest correlations for SAR data were found between forest AGB and the annual images, followed by the hot season, and least for the rainy season. We observed a larger correlation between forest AGB and the dry season images, followed by the annual images and, lastly, the hot season images for optical data. These correlation results are similar to those obtained by other studies (Fagua et al., 2019; Li et al., 2020; Chen et al., 2023).

3.3 SAR and optical predictor variable importance

Fig. 5 shows the predictor variable importance for the four models that used SAR data alone. The raw polarisation bands were the best predictors for all models, with VH as the most important variable except for the rainy season. There was no consistency with the texture variables. The quotient, VV/VH appeared consistently among the best 10 predictor variables for all four models.

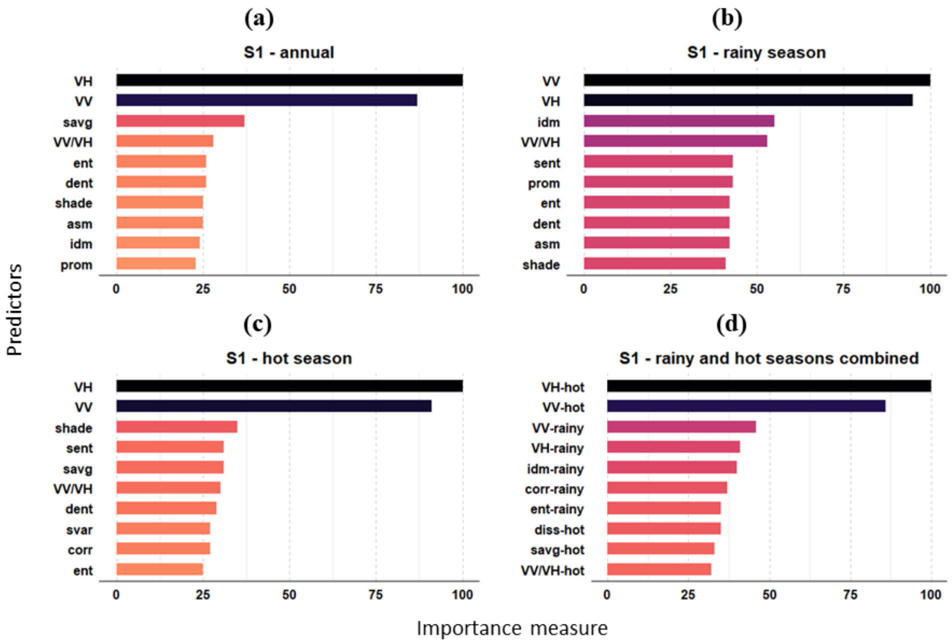

Fig. 5. Variable importance charts of forest AGB models that used SAR data alone.

Fig. 6 shows the predictor variable importance for the four models that used optical data alone. Spectral bands were more important predictors of forest AGB compared to vegetation indices and texture bands for the dry season. Vegetation indices were more important predictors than the spectral bands for the hot season. When the dry and hot season images were combined, the spectral bands from the dry season were more important predictors than the vegetation indices from the hot season images.

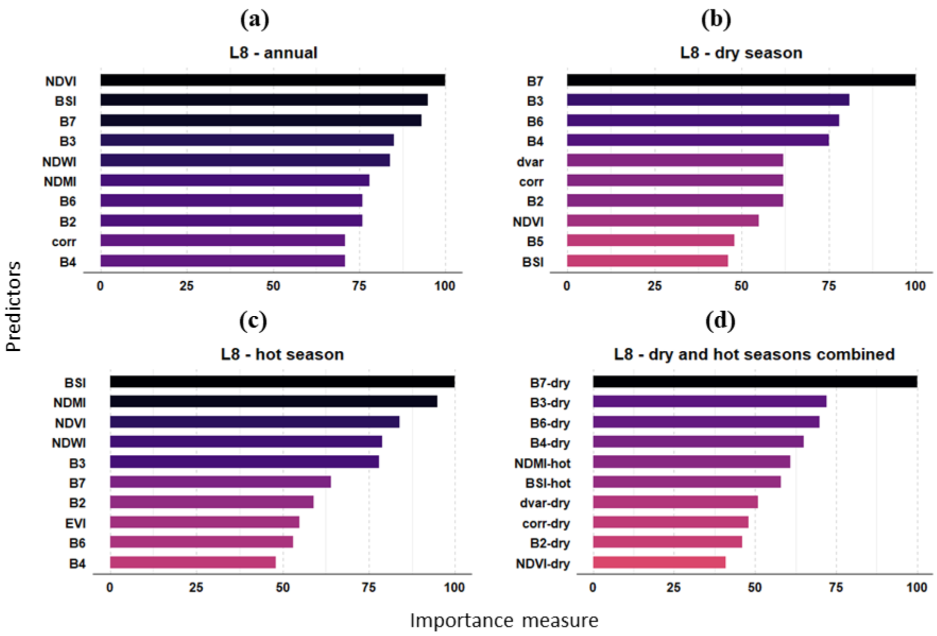

Fig. 6. Variable importance of forest AGB models that used optical data alone.

Fig. 7 shows the predictor variable importance for the three models that combined SAR and optical data. The VH band was the most important predictor variable in all three models. The model showed spectral bands from the dry season as more important forest AGB predictor variables compared to vegetation indices.

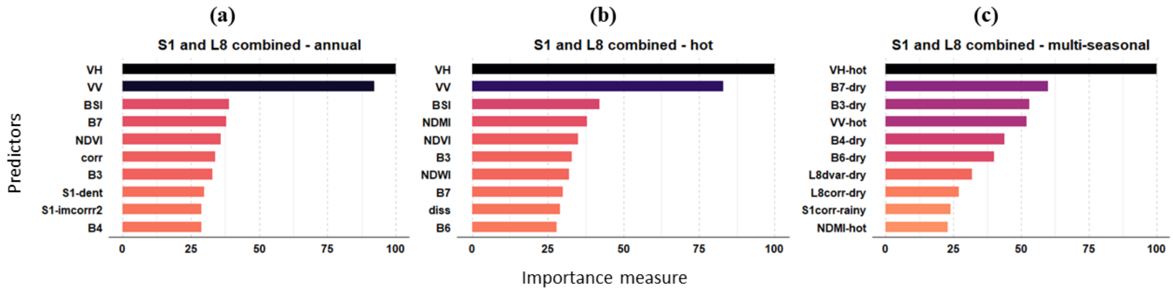

Fig. 7. Variable importance of forest AGB models that used SAR and optical data combined.

3.4 Forest AGB models of SAR, Optical and SAR-Optical data combined

Tables 2 and 3 show the regression modelling results obtained from all 55 models fitted in this research based on validation data and Tables S10 and S11 are based on training data.

3.4.1 AGB models based on the entire study area

When we compared time periods, the most accurate prediction with SAR data was achieved using the annual images, followed by the hot season, and lastly the rainy season images, while for optical data the most accurate prediction was achieved using the dry season images, followed by the hot season images, with the annual images being the least accurate.

Table 2

Forest AGB model validation results for the 11 models based on entire study area (142 plots)

Model	Abbreviation	R	MAE	RMSE	SMAPE
SAR-rainy	S1-r	0.30	19.24	23.65	0.65
SAR-hot	S1-h	0.55	15.79	20.60	0.57
SAR-rainy and hot	S1-r & h	0.61	15.38	19.64	0.58
SAR-annual	S1-y	0.59	15.80	19.92	0.60
Optical-dry	L8-d	0.55	15.98	20.55	0.59
Optical-hot	L8-h	0.54	16.12	20.81	0.61
Optical-dry and hot	L8 d & h	0.62	14.94	19.45	0.58
Optical-annual	L8-y	0.51	16.55	21.31	0.61
SAR and Optical-hot	S1L8-hot	0.65	14.41	18.80	0.56
SAR and Optical-multi-season	S1L8-m	0.69	14.01	18.23	0.55
SAR and Optical-annual	S1L8-y	0.61	15.45	19.65	0.59

Combining the seasonal images predicted forest AGB more accurately compared to using single season and annual images for both SAR and optical data. In this case, using optical data was more accurate than using SAR images with an R of 0.62 compared to 0.61 and RMSE of 19.45 Mg ha^{-1} compared to 19.65 Mg ha^{-1} respectively.

Combining SAR and optical data increased the prediction accuracy compared to using the individual datasets. Multi-seasonal SAR and optical images produced the smallest RMSE of 18.23 Mg ha^{-1} and largest correlation (R = 0.69). Fig. 8 shows scatterplots of the observed against predicted forest AGB based on the NFI validation data.

In terms of SMAPE, the prediction accuracies were ordered as follows: SAR and optical multi-seasonal at 0.55, SAR and optical hot season at 0.56, SAR hot season at 0.57, SAR rainy and hot seasons at 0.58, optical dry and hot seasons at 0.58, SAR and optical annual at 0.59, optical dry season at 0.59, SAR annual at 0.60, optical hot season at 0.61, optical annual at 0.61 and SAR rainy season at 0.65.

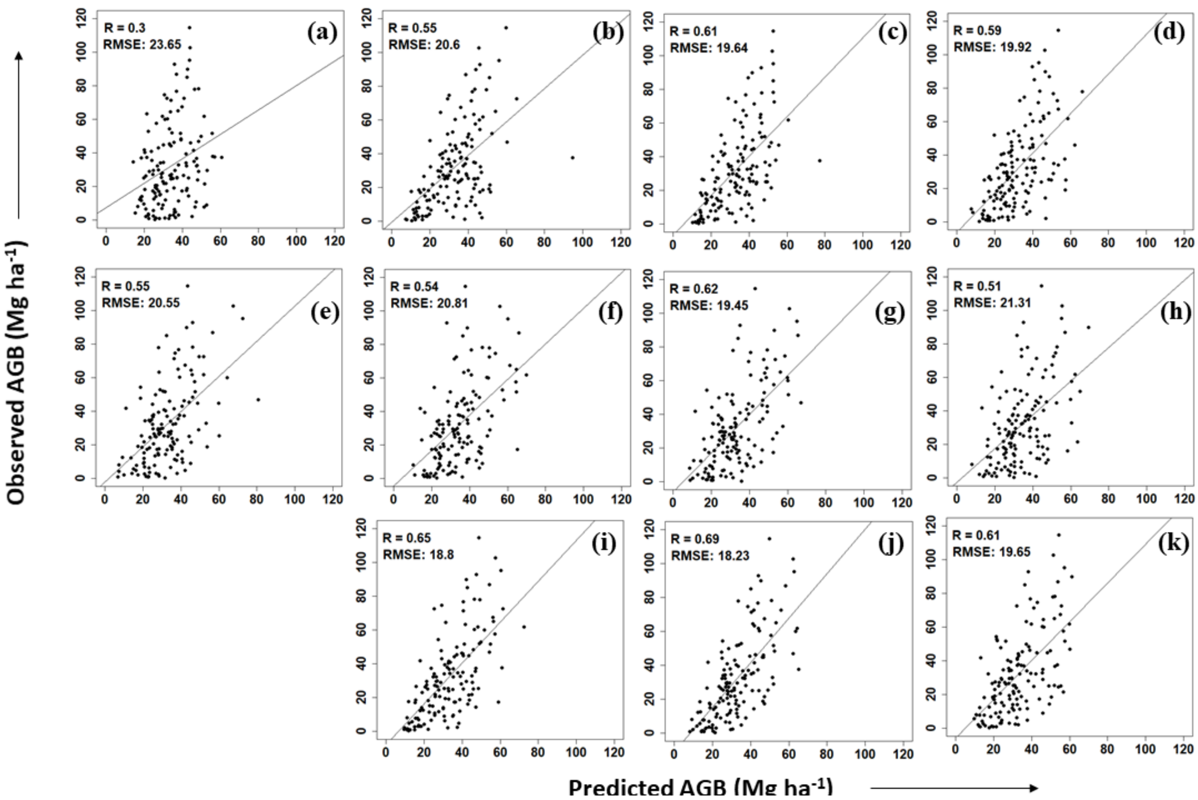

Fig 8. Scatterplots of observed against predicted forest AGB in Mg ha^{-1} for the 11 models based on the entire study area using the 15% NFI validation dataset: (a) SAR rainy season model, (b) SAR hot season model, (c) SAR rainy and hot, (d) SAR annual, (e) optical dry season, (f) optical hot season, (g) optical dry and hot, (h) optical annual, (i) SAR and optical hot season, (j) SAR and optical multi-season and (k) SAR and optical annual.

3.4.2 Forest AGB models based on individual agro-ecological zones

We observed an increased forest AGB prediction accuracy when we considered agro-ecological zones as the individual study units, especially for agro-ecological zones I and III (Table 3).

For agro-ecological zone I, large correlations between observed and predicted forest AGBs were observed in most models, with the one that combined SAR and optical annual images producing a very large correlation. Annual images for both SAR and optical images were more useful than seasonal images in this zone. Overall, optical data produced higher accuracy than SAR data in this agro-ecological zone.

For agro-ecological zone IIa, the largest correlation was observed for the model that combined SAR and optical annual images. In this zone, optical data produced greater accuracy than the SAR data.

For agro-ecological zone IIb, we observed a moderate correlation across all 11 models. The largest correlation was recorded for the model that combined the rainy and hot season SAR images. In this zone, the SAR data produced a greater accuracy than the optical data.

For agro-ecological zone III, a generally larger correlation in all 11 models was observed compared to the other zones. SAR and optical competed favourably in predicting forest AGB.

Table 3

Forest AGB model validation results for 11 models replicated across the four agro-ecological zones. Agro-eco I (26 plots), Agro-eco IIa (47 plots), Agro-eco IIb (31 plots) and Agro-eco III (37 plots). RMSE (Mg ha^{-1}).

Model	Agro-eco I		Agro-eco IIa		Agro-eco IIb		Agro-eco III	
	R	RMSE	*R*	RMSE	*R*	RMSE	*R*	RMSE
S1-rainy	0.32	30.83	0	22.84	0.46	30.05	0.14	30.85
S1-hot	0.41	29.69	0.32	19.80	0.44	32.11	0.81	18.06
S1-rainy and hot	0.55	28.18	0.32	19.41	0.53	31.00	0.78	19.30
S1-annual	0.61	26.58	0.41	18.67	0.45	31.81	0.64	22.67
L8-dry	0.61	26.88	0.28	19.61	0.48	31.17	0.62	23.15
L8-hot	0.27	31.18	0.33	19.01	0.39	32.72	0.60	23.90
L8 dry and hot	0.63	27.15	0.42	18.17	0.42	32.15	0.67	22.41
L8-annual	0.71	25.66	0.42	18.50	0.42	32.16	0.71	21.47
S1L8-hot	0.39	29.85	0.4	18.63	0.45	31.74	0.77	19.71
S1L8-multi-season	0.73	26.31	0.43	18.17	0.49	31.21	0.78	19.33
S1L8-annual	0.75	24.61	0.44	18.37	0.44	31.83	0.79	18.93

Fig. 9 shows a visual comparison of forest AGB estimation with optical data alone, SAR data alone and their synergy and with ESA biomass climate change initiative. The optimal models for SAR (S1 rainy & hot), optical (L8 dry & hot) and their synergy (S1L8 multi-season) were used to produce these forest AGB maps. The map produced from SAR and optical multi-seasonal images appears to be in accordance with the shortwave infrared image, with larger forest AGB values shown in dark green. The map produced from the optical images appears to identify the areas with small forest AGB values, but misses areas with larger forest AGB values, while the opposite is true for the map produced from SAR images. The global biomass map by ESA appears to underestimate lower values of AGB while at the same time overestimating higher values of AGB compared to this research.

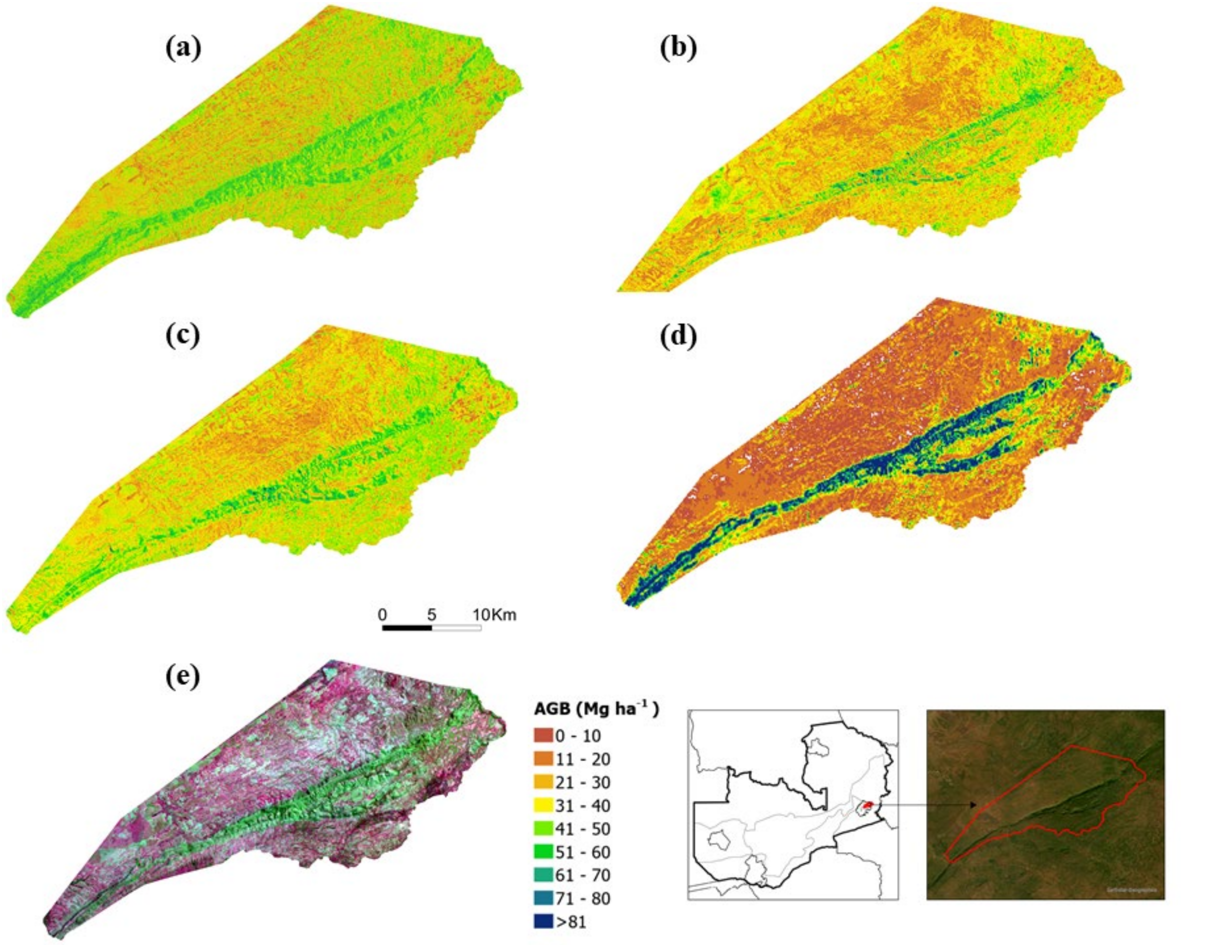

Fig. 9. Forest AGB maps produced from optimal models comparing (a) SAR alone, (b) Optical alone, (c) SAR and optical combined, (d) ESA Biomass Climate Change Initiative AGB for 2015 (e) Shortwave Infrared 753 L8 image for the Machinje Hills national forest reserve in Mambwe District.

3.5 Spatial distribution of modelled forest AGB across four agro-ecological zones

Fig. 10 shows the spatial distribution of modelled forest AGB across four agro-ecological zones in Zambia using the S1-L8 multi-seasonal model, developed based on the entire study area. The model was trained using all 951 NFI plots. The model diagnostic errors are presented in Table S12. We sampled one district to represent each agro-ecological zone.

The model-predicted District wall-to-wall forest AGB maps are consistent with the NFI data. Model predicted mean AGB was 38.08 Mg ha^{-1} against the NFI plot AGB of 41.98 Mg ha^{-1} for Kawambwa, 22.18 Mg ha^{-1} against 25.42 Mg ha^{-1} for Mongu, 36.18 Mg ha^{-1} against 29.70 Mg ha^{-1} for Mambwe and 31.95 Mg ha^{-1} against 24.76 Mg ha^{-1} for Kazungula (Table S13).

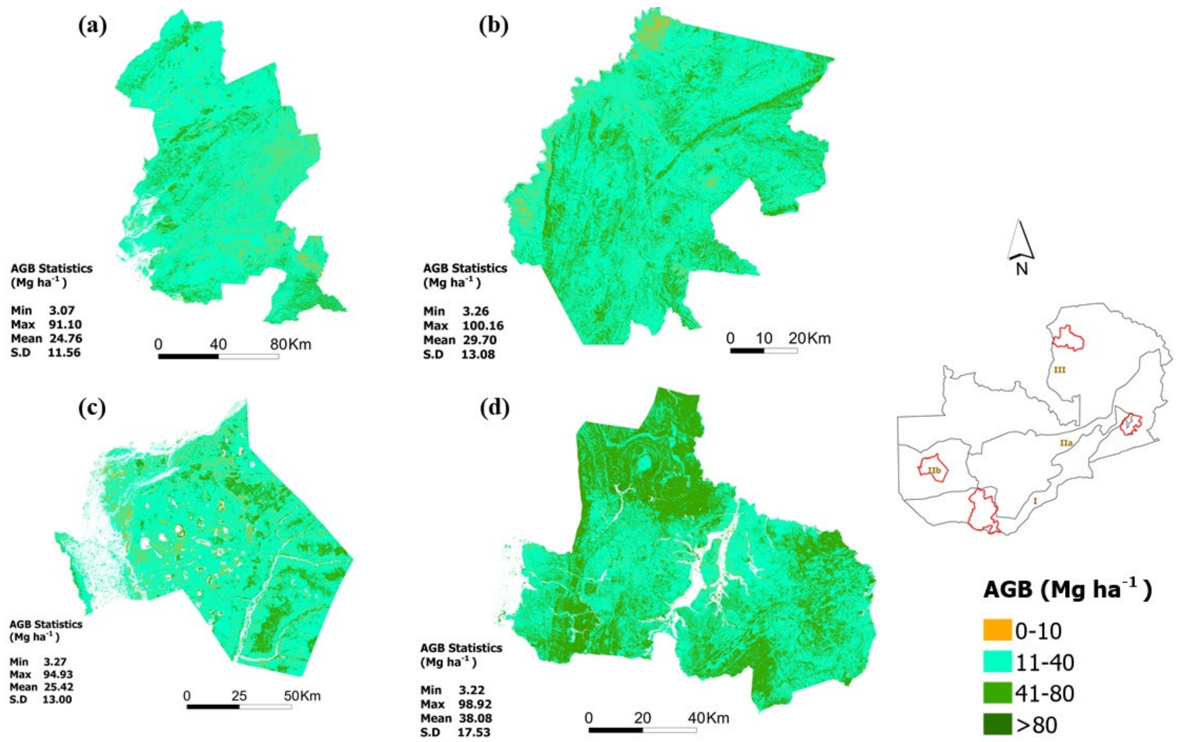

Fig. 10. Modelled forest AGB wall-to-wall maps of four Districts representing the four agro-ecological zones in Zambia. (a) Kazungula District – agro-ecological zone I, (b) Mambwe District – agro-ecological zone IIa, (c) Mongu District – agro-ecological zone IIb and (d) Kawambwa – agro-ecological zone III.

4 Discussion

4.1 Effectiveness of SAR images for forest AGB estimation

SAR backscattering is affected by features that constitute the plant macro-structure such as leaves, branches, and trunks (Jones and Vaughan, 2010). SAR backscatter is also dependant on the size, shape, orientation, and water content of green leaves (Jones and Vaughan, 2010; Ghosh and Behera, 2018). A positive correlation between forest AGB and SAR was reported in previous studies (Kuplich et al., 2005; McNicol et al., 2018b; David et al., 2022a).

In the current research, we assessed the effectiveness of SAR data when used alone and when combined with optical data for forest AGB estimation in a tropical dry forest dominated by Miombo woodlands. HV polarisation from Sentinel-1 C band was found to be the most accurate predictor variable for forest AGB as observed in all the models that used it. Other similar studies found forest AGB of Miombo woodlands to correlate well with HV backscatter (Mitchard et al., 2009; Mitchard et al., 2013a; Gou et al., 2019), across four different African landscapes (Navarro et al., 2019). To the contrary, David et al. (2022) found forest AGB to be more correlated with VV polarisation for a similar dry forest but using an image from the rainy season. They justified the minimum influence of rainfall and soil moisture on the backscatter because their image was acquired during a period when there was drought. Our results from correlation analysis, as well as variable importance analysis, for SAR-rainy season concur with

David et al. (2022) where VV and VH produced similar correlations with forest AGB, and where VV was a slightly more accurate predictor compared to VH. Because our study was spatially extensive, with many sample plots across different ecological zones, and it also considered seasonal images, we confirm that the VH polarisation of Sentinel-1 is generally a more accurate predictor of forest AGB than the VV polarisation for the dry forests of Southern Africa such as the Miombo woodlands. Our findings can be attributed to the fact that cross-polarised SAR (VH) is associated with measuring volume scattering (biomass) while co-polarised SAR (VV) is associated with surface scattering (Flores-Anderson et al., 2019).

Overall, our model results show that Sentinel-1 SAR data compare favourably with Landsat-8 optical data in predicting forest AGB for Zambia's Miombo woodlands when single time periods are considered. Similar studies have reported SAR to be a more accurate predictor compared to optical data (Lu Zhang, 2019; David et al., 2022a) contrary to other similar studies (Li et al., 2020; Zimbres et al., 2021; Qadeer et al., 2024). The higher accuracy of SAR compared to optical data can be attributed to the closed, but not-so-dense canopy of the Miombo woodlands, thereby, making SAR interactions with tree leaves, branches and trunks informative. The *C*-band from Sentinel-1 SAR, although having a shorter wavelength compared with the *L* and *P* bands, is suitable for less dense forests such as the Miombo woodlands. David et al. (2022) reported a similar result for the tropical dry forests of Botswana, a neighbouring country to Zambia. However, combined seasonal images for Landsat-8 (dry and hot season images) were more accurate predictors of forest AGB compared to combined seasonal images for Sentinel-1 (rainy and hot season images). Combining SAR and optical data produced the highest accuracy, similar to other studies that combined SAR and optical images for forest AGB estimation (Cutler et al., 2012; Forkuor et al., 2020; David et al., 2022a).

4.2 Seasonal effects of remote sensing data on forest AGB estimation

The model results show that annual SAR images predicted forest AGB more accurately than the hot season and rainy season images, but combining the rainy and hot season images surpassed the accuracy achieved using annual images. The rainy season images were the least accurate. Other studies reported similar results with SAR data performing poorly, and with less accurate forest AGB estimation for the rainy season when water content is high in the soil and leaves (Forkuor et al., 2020; Chen et al., 2023). We anticipated that a larger correlation would exist between forest AGB and SAR during the rainy season because vegetation is at its peak production during this season. However, our results suggest that the higher soil water content and greater vegetation cover that characterise the rainy season leads to increased vegetation water content and this, coupled with the relatively short wavelength SAR *C*-band used, leads to reduced sensitivity of SAR to forest AGB as backscatter from the canopy is enhanced. Also, the dielectric constant is higher in the rainy season (increased canopy backscattering) due to increased water content in soils and vegetation. Therefore, vegetation amount, which changes with the seasons, has a large effect on SAR backscattering and, thus, the predictive ability of the SAR images. For example, a larger correlation was recorded when using the hot season images, as this season is characterised by dry and open crowns with leaves just beginning to appear, thereby, exposing branches and trunks (Laurin et al., 2018). This might explain why combining Sentinel-1 SAR data from different seasons predicted more accurately. It would be interesting to note how Sentinel-1 SAR data perform in the dry season, when Sentinel-1 SAR dry season images are available.

For the optical data, the dry season images produced the largest correlations between the observed and predicted forest AGB, followed by the hot season images, and lastly the annual images. These results conform with other studies that reported large correlations when dry season images were used (Halperin et al., 2016a; Macave et al., 2022; Chen et al., 2023). The dry season occurs immediately after the rainy season when the trees shed their leaves, and leaf litter and grass senesce. The greater accuracy attained when using dry season images could be attributed to exposure of branches and trunks which store carbon and, therefore, reflectance coming directly from branches and trunks with little effect of leaves. Additionally, the dry season is mostly clear with minimal cloud cover and aerosol effects that affect the image quality as compared to the hot season (and annual images).

Combining images of different seasons, whether single sensor or combined, produced greater forest AGB estimation accuracies compared to the annual images, similar to the findings from previous studies (Rodriguez-Galiano et al., 2012; Laurin et al., 2018; Chen et al., 2023). This can be attributed to the richness of vegetation phenology information that is captured in seasonal images as reported in similar studies (Castillo et al., 2017; Chen et al., 2023).

4.3 Performance of forest AGB models across the four agro-ecological zones

The accuracy of the 11 models across the four agro-ecological zones varied. This is as expected due to the distinctive climatic conditions, topography, soil and terrain, which affect the predominant vegetation types as well as tree growth patterns.

For agro-ecological zone I, correlations (R) between the observed and predicted forest AGB of above 0.70 were recorded for models that used annual optical images, combined annual optical and SAR images, and combined seasonal optical and SAR images. The greater performance of optical data over SAR data in this agro-ecological zone can be attributed to the lower tree density that characterise this zone. SAR data have been reported to be inaccurate on heavily disturbed/sparse forests (Nicolau et al., 2021). This zone is dominated by Mopane woodlands and dry Miombo woodlands. *Colophospermum mopane*, the dominant tree in this Mopane woodland, is an adapted tree species capable of withstanding drought, low nutrients and disturbances (Makhado et al., 2014). However, despite the low tree density, the sampled plots from the Mopane woodlands had a large mean forest AGB (Mg ha^{-1}), indicating the presence of some sparsely distributed, but very large trees. The drought resistant adaptability coupled with lower tree density, and propensity for mixed pixels, might explain why forest AGB had a small correlation with both the SAR and optical data in this zone. Halperin et al. (2016) also noted an irregular pattern where a large range of observed forest AGB corresponded to smaller observed values of vertical canopy cover for the Mopane woodlands (Halperin et al., 2016a).

Agro-ecological zone IIa is dominated by Miombo woodlands and Hill (Miombo) woodlands. The relatively low accuracy of our predictor variables in this zone might be because of the terrain, as this zone includes mountains and valleys. For example, Li et al. (2020) reported low accuracies using SAR data due to the terrain. The other reason for small correlations between observed forest AGB and SAR/optical data in agro-ecological zone IIa is that forest patches lead to mixed pixels, as this zone is reported to experience substantial encroachment by agricultural expansion and charcoal burning (Kanja et al., 2019b; Phiri et al., 2023).

Agro-ecological zone IIb, dominated by Kalahari (47%) and Miombo (37%) woodlands, showed moderate correlations, evident when observed forest AGB was plotted against predicted forest AGB. This zone has a stable terrain with elevation ranging from 1000 m to 1200 m above sea level.

Agro-ecological zone III, which is dominated by wet Miombo woodlands (87% of the sample plots), showed very large correlations between observed and predicted forest AGB. A similar observation was made by Halperin et al. (2016) who reported a more regular pattern for the Miombo woodlands compared to other vegetation types when they plotted forest AGB against canopy cover. Both SAR and optical predictors correlated well with forest AGB in this zone. The high predictive accuracy of SAR can be attributed to the structure of the vegetation canopy for Miombo woodlands, with fewer canopy overlaps, thereby allowing the C-band SAR to penetrate and interact optimally with the vegetation canopy, producing a high local variance in the observed forest AGB. Pham et al. (2019) also reported the usefulness of Sentinel-1A images for biomass estimation and mapping in tropical forest types.

4.4 Future research

Future research should consider stratifying the forest into distinct classes, to increase the estimation accuracy of forest AGB for the Miombo woodlands using remote sensing data from space combined with NFI data. Previous studies that utilised SAR, optical and combinations of both types of imagery to map the Miombo woodlands (McNicol et al., 2018b; Macave et al., 2022; David et al., 2022a) used single date remote sensing data. The current study explored the seasonal variation of SAR/optical imagery to increase the accuracy of AGB estimation. The datasets available for the analysis were limited in some seasons (e.g., optical for the rainy season and SAR for the dry season). We recommend exploring the use of finer temporal resolution optical data such as from Sentinel-2 and using commercial SAR data where available. Global LiDAR datasets such as global ecosystem dynamic investigation (GEDI) should be explored while paying attention to their local calibration (Liang et al., 2023; Li et al., 2024). The spectral unmixing of mixed pixels, especially when working with medium spatial resolution images such as Landsat images, and in areas where tree density is low, such as in agro-ecological zone I, may help increase the estimation accuracy of forest AGB from space. Inclusion of auxiliary variables such as elevation, proximity to developed infrastructure (such as roads) and protection status might also help to increase prediction model accuracies, as reported in other similar studies (Halperin et al., 2016a; Liu et al., 2024).

5 Conclusion

This research used extensive NFI data in Zambia to evaluate the potential of SAR and optical data for estimating the forest AGB of Miombo woodlands. We compared the effectiveness of SAR and optical data when used independently and when combined. We also assessed the efficacy of SAR and optical images in different seasons. A multi-level experiment involving 11 models was developed to address the objectives of this research. The 11 models were replicated across four agro-ecological zones found in Zambia, resulting in 44 models, to evaluate the impact of climatic and environmental variation on the results.

The models that used combined seasonal images produced greater accuracy compared to single season images and annual images. For SAR data, the annual images produced greater accuracy than the hot season and rainy season images. For optical data, the dry season images led to greater accuracy than the hot season and annual images. The SAR VH band was the most accurate predictor variable for all the models that used SAR data alone or combined with optical data. Spectral bands were more accurate predictors of forest AGB using the dry season images, while vegetation indices were more accurate predictors of forest AGB using the hot season images.

We conclude that considering seasonal effects is important when using SAR and optical images for forest AGB estimation in the Miombo woodlands. Combining SAR bands from the hot season, optical bands from the dry season and vegetation indices from the hot season produced the most accurate forest AGB estimation model for the present study in Zambia. However, the 11 models representing different data combinations performed differently across the four agro-ecological zones. This implies that both SAR and optical images interact differently with the different vegetation cover types in Zambia. We recommend that the ongoing REDD+ carbon projects in Zambia and other countries in southern Africa adopt the findings of this research where seasonal effects are considered when selecting satellite sensor imagery (in particular, using SAR and optical data from different seasons) for mapping the forest AGB of the Miombo woodlands.

Author Contributions

KK, CZ and PMA conceived the idea and designed the methodology for the study. KK designed the experimental approach. KK analysed the data and drafted the manuscript with supervision from CZ and PMA. CZ and PMA critically reviewed and edited the manuscript. All authors approved the final draft manuscript for submission to the journal.

Declaration of competing interest

The authors declare no known competing interest, either personal relations or financial interests, that could have influenced the work reported in this research.

Data Availability Statement

Inventory data and remote sensing data together with codes used in this study will be made available upon request.

Acknowledgement

We thank the Commonwealth Scholarship Commission who provided funding for KK's Environmental Science doctoral training program at Lancaster University, PhD grant number: ZMCS-2021-536, for the period 2021 to 2024. We are grateful to the Forestry Department of Zambia for providing the National Forest Inventory data used in this research, which were collected during the ILUA II project.

References

Atkinson, P. M., Foody, G. M., Curran, P. J. & Boyd, D. S., 2000. Assessing the ground data requirements for regional scale remote sensing of tropical forest biophysical properties. *Int. J. Remote Sens.* 21(13-14), 2571-2587. 10.1080/014311600050110188.

Bouvet, A., Mermoz, S., Le Toan, T., Villard, L., Mathieu, R., Naidoo, L. & Asner, G. P., 2018. An above-ground biomass map of African savannahs and woodlands at 25 m resolution derived from ALOS PALSAR. *Remote Sens. Environ.* 206, 156-173. 10.1016/j.rse.2017.12.030.

Breiman, L., 2001. Random forests. *Machine learning* 45(1), 5-32. 10.1023/A:1010933404324.

Bulusu, M., Martius, C. & Clendenning, J., 2021. Carbon stocks in miombo woodlands: Evidence from over 50 years. *For.* 12(7), 862. 10.3390/f12070862.

Campbell, B. M.,1996. *The Miombo in transition: woodlands and welfare in Africa.* Cifor.

Carreiras, J. M. B., Vasconcelos, M. J. & Lucas, R. M., 2012. Understanding the relationship between aboveground biomass and ALOS PALSAR data in the forests of Guinea-Bissau (West Africa). *Remote Sens. Environ.* 121, 426-442. 10.1016/j.rse.2012.02.012.

Cartus, O. & Santoro, M., 2019. Exploring combinations of multi-temporal and multi-frequency radar backscatter observations to estimate above-ground biomass of tropical forest. *Remote Sens. Environ.* 232, 111313. 10.1016/j.rse.2019.111313.

Cassells, G. F., Woodhouse, I. H., Mitchard, E. T. A. & Tembo, M. D., The use of ALOS PALSAR for supporting sustainable forest use in southern Africa: A case study in Malawi. *2009 IEEE International Geoscience and Remote Sensing Symposium*. IEEE, II-206-II-209.

Castillo, J. a. A., Apan, A. A., Maraseni, T. N. & Salmo, S. G., 2017. Estimation and mapping of above-ground biomass of mangrove forests and their replacement land uses in the Philippines using Sentinel imagery. *ISPRS J. Photogramm. Remote Sens.* 134, 70-85. 10.1016/j.isprsjprs.2017.10.016.

Chave, J., Réjou-Méchain, M., Búrquez, A., Chidumayo, E., Colgan, M. S., Delitti, W. B. C., Duque, A., Eid, T., Fearnside, P. M., Goodman, R. C., Henry, M., Martínez-Yrízar, A., Mugasha, W. A., Muller-Landau, H. C., Mencuccini, M., Nelson, B. W., Ngomanda, A., Nogueira, E. M., Ortiz-Malavassi, E., Pélissier, R., Ploton, P., Ryan, C. M., Saldarriaga, J. G. & Vieilledent, G., 2014. Improved allometric models to estimate the aboveground biomass of tropical trees. *Glob. Chang. Biol.* 20(10), 3177-3190. 10.1111/gcb.12629.

Chen, C., He, Y., Zhang, J., Xu, D., Han, D., Liao, Y., Luo, L., Teng, C. & Yin, T., 2023. Estimation of Above-Ground Biomass for Pinus densata Using Multi-Source Time Series in Shangri-La Considering Seasonal Effects. *For.* 14(9), 1747. 10.3390/f14091747.

Chidumayo, E. N.,2012. Assessment of Existing Models for Biomass and Volume Calculations for Zambia. Report Prepared for FAO-Zambia Integrated Land Use Assessment (ILUA) Phase II Project.

Chidumayo, E. N., 2013. Forest degradation and recovery in a miombo woodland landscape in Zambia: 22 years of observations on permanent sample plots. *For. Ecol. Manag.* 291, 154-161. 10.1016/j.foreco.2012.11.031.

Chidumayo, E. N. & Gumbo, D. J.,2010. *The dry forests and woodlands of Africa : managing for products and services.* London: Earthscan.

Chrysafis, I., Mallinis, G., Tsakiri, M. & Patias, P., 2019. Evaluation of single-date and multi-seasonal spatial and spectral information of Sentinel-2 imagery to assess growing stock volume of a Mediterranean forest. *Int. J. Appl. Earth Obs. Geoinf.* 77**,** 1-14. 10.1016/j.jag.2018.12.004.

Cutler, M. E. J., Boyd, D. S., Foody, G. M. & Vetrivel, A., 2012. Estimating tropical forest biomass with a combination of SAR image texture and Landsat TM data: An assessment of predictions between regions. *ISPRS J. Photogramm. Remote Sens.* 70**,** 66-77. 10.1016/j.isprsjprs.2012.03.011.

David, R. M., Rosser, N. J. & Donoghue, D. N. M., 2022a. Improving above ground biomass estimates of Southern Africa dryland forests by combining Sentinel-1 SAR and Sentinel-2 multispectral imagery. *Remote Sens. Environ.* 282**,** 113232. 10.1016/j.rse.2022.113232.

David, R. M., Rosser, N. J. & Donoghue, D. N. M., 2022b. Remote sensing for monitoring tropical dryland forests: a review of current research, knowledge gaps and future directions for Southern Africa. *Environ. Res. Commun.* 4(4)**,** 042001. 10.1088/2515-7620/ac5b84.

Demol, M., Aguilar-Amuchastegui, N., Bernotaite, G., Disney, M., Duncanson, L., Elmendorp, E., Espejo, A., Furey, A., Hancock, S., Hansen, J., Horsley, H., Langa, S., Liang, M., Locke, A., Manjate, V., Mapanga, F., Omidvar, H., Parsons, A., Peneva-Reed, E., Perry, T., Puma Vilca, B. L., Rodríguez-Veiga, P., Sutcliffe, C., Upham, R., De Walque, B. & Burt, A., 2024. Multi-scale lidar measurements suggest miombo woodlands contain substantially more carbon than thought. *Commun. Earth Environ.* 5(1)**,** 366-11. 10.1038/s43247-024-01448-x.

Egberth, M., Nyberg, G., Næsset, E., Gobakken, T., Mauya, E., Malimbwi, R., Katani, J., Chamuya, N., Bulenga, G. & Olsson, H., 2017. Combining airborne laser scanning and Landsat data for statistical modeling of soil carbon and tree biomass in Tanzanian Miombo woodlands. *Carbon Balanc. Manag.* 12(1)**,** 8-8. 10.1186/s13021-017-0076-y.

Fagua, J. C., Jantz, P., Rodriguez-Buritica, S., Duncanson, L. & Goetz, S. J., 2019. Integrating LiDAR, multispectral and SAR data to estimate and map canopy height in tropical forests. *Remote Sens. (Basel, Switzerland)* 11(22)**,** 2697. 10.3390/rs11222697.

Flores-Anderson, A., K., H., Rajesh, T. & Emil, C.,2019. *SAR Handbook: Comprehensive Methodologies for Forest Monitoring and Biomass Estimation.* 10.25966/nr2c-s697.

Forkuor, G., Benewinde Zoungrana, J.-B., Dimobe, K., Ouattara, B., Vadrevu, K. P. & Tondoh, J. E., 2020. Above-ground biomass mapping in West African dryland forest using Sentinel-1 and 2 datasets - A case study. *Remote Sens. Environ.* 236**,** 111496. 10.1016/j.rse.2019.111496.

Gascón, L. H., Ceccherini, G., Haro, F. J. G., Avitabile, V. & Eva, H., 2019. The potential of high resolution (5 m) RapidEye optical data to estimate above ground biomass at the national level over Tanzania. *For.* 10(2)**,** 107. 10.3390/f10020107.

Ghosh, S. M. & Behera, M. D., 2018. Aboveground biomass estimation using multi-sensor data synergy and machine learning algorithms in a dense tropical forest. *Appl. Geogr. (Sevenoaks)* 96**,** 29-40. 10.1016/j.apgeog.2018.05.011.

Gizachew, B., Solberg, S., Næsset, E., Gobakken, T., Bollandsås, O. M., Breidenbach, J., Zahabu, E. & Mauya, E. W., 2016. Mapping and estimating the total living biomass and carbon in low-biomass woodlands using Landsat 8 CDR data. *Carbon Balanc. Manag.* 11(1)**,** 1-14. 10.1186/s13021-016-0055-8.

Gou, Y., Ryan, C. & Balzter, H., Water Cloud Model for Above Ground Biomass retrieval in Savanna woodlands. *IGARSS 2019 - 2019 IEEE International Geoscience and Remote Sensing Symposium*. Yokohama, Japan. 6011–6014.

Halperin, J., Lemay, V., Chidumayo, E., Verchot, L. & Marshall, P., 2016a. Model-based estimation of above-ground biomass in the miombo ecoregion of Zambia. *For. Ecosyst.* 3(1). 10.1186/s40663-016-0077-4.

Halperin, J., Lemay, V., Coops, N., Verchot, L., Marshall, P. & Lochhead, K., 2016b. Canopy cover estimation in miombo woodlands of Zambia: Comparison of Landsat 8 OLI versus RapidEye imagery using parametric, nonparametric, and semiparametric methods. *Remote Sens. Environ.* 179, 170-182. 10.1016/j.rse.2016.03.028.

Handavu, F., Syampungani, S., Sileshi, G. W. & Chirwa, P. W. C., 2021. Aboveground and belowground tree biomass and carbon stocks in the miombo woodlands of the Copperbelt in Zambia. *Carbon Manag.* 12(3), 307-321. 10.1080/17583004.2021.1926330.

Harris, N. L., 2012. Baseline map of carbon emissions from deforestation in tropical regions (Science (1573)). *Science (American Association for the Advancement of Science)* 337(6091), 155-155. 10.1126/science.337.6091.155-b.

Herold, M., Carter, S., Avitabile, V., Espejo, A. B., Jonckheere, I., Lucas, R., Mcroberts, R. E., Næsset, E., Nightingale, J., Petersen, R., Reiche, J., Romijn, E., Rosenqvist, A., Rozendaal, D. M. A., Seifert, F. M., Sanz, M. J. & Sy, D. V., 2019. The Role and Need for Space-Based Forest Biomass-Related Measurements in Environmental Management and Policy. *Surv. Geophys.* 40(4), 757-778. 10.1007/s10712-019-09510-6.

Jones, H. G. & Vaughan, R. A.,2010. *Remote sensing of vegetation : principles, techniques, and applications.* New York: Oxford University Press.

Joshi, N., Baumann, M., Ehammer, A., Fensholt, R., Grogan, K., Hostert, P., Jepsen, M. R., Kuemmerle, T., Meyfroidt, P., Mitchard, E. T. A., Reiche, J., Ryan, C. M. & Waske, B., 2016. A review of the application of optical and radar remote sensing data fusion to land use mapping and monitoring. *Remote Sens. (Basel, Switzerland)* 8(1), 70. 10.3390/rs8010070.

Kalaba, F. K., Quinn, C. H. & Dougill, A. J., 2013. Contribution of forest provisioning ecosystem services to rural livelihoods in the Miombo woodlands of Zambia. *Popul. Environ.* 35(2), 159-182. 10.1007/s11111-013-0189-5.

Kanja, K., Karahalil, U. & Çil, B., 2019a. Modeling stand parameters for <i>Pinus brutia</i> (Ten.) using airborne LiDAR data: a case study in Bergama. *J. Appl. Remote Sens.* 14(2), 022205.

Kanja, K., Mwemba, M. & Malunga, K., 2019b. Monitoring the rate of expansion of agricultural fields in Mwekera forest reserve using remote sensing and GIS. *Int. Arch. photogramm. Remote Sens. Spat. Inf. Sci.* XLII-3/W6, 377-380. 10.5194/isprs-archives-XLII-3-W6-377-2019.

Kuplich, T. M., Curran, P. J. & Atkinson, P. M., 2005. Relating SAR image texture to the biomass of regenerating tropical forests. *Int. J. Remote Sens.* 26(21), 4829-4854. 10.1080/01431160500239107.

Laurin, G. V., Balling, J., Corona, P., Mattioli, W., Papale, D., Puletti, N., Rizzo, M., Truckenbrodt, J. & Urban, M., 2018. Above-ground biomass prediction by Sentinel-1 multitemporal data in central Italy with integration of ALOS2 and Sentinel-2 data. *J. Appl. Remote Sens.* 12(1). 10.1117/1.JRS.12.016008.

Li, X., Wessels, K., Armston, J., Duncanson, L., Urbazaev, M., Naidoo, L., Mathieu, R. & Main, R., 2024. Evaluation of GEDI footprint level biomass models in Southern African

Savannas using airborne LiDAR and field measurements. *Sci. Remote Sens.* 10, 100161. 10.1016/j.srs.2024.100161.

Li, Y., Li, M., Li, C. & Liu, Z., 2020. Forest aboveground biomass estimation using Landsat 8 and Sentinel-1A data with machine learning algorithms. *Sci. Rep.* 10(1), 9952-12. 10.1038/s41598-020-67024-3.

Liang, M., Duncanson, L., Silva, J. A. & Sedano, F., 2023. Quantifying aboveground biomass dynamics from charcoal degradation in Mozambique using GEDI Lidar and Landsat. *Remote Sens. Environ.* 284, 113367. 10.1016/j.rse.2022.113367.

Liu, Z., Long, J., Lin, H., Sun, H., Ye, Z., Zhang, T., Yang, P. & Ma, Y., 2024. Mapping and analyzing the spatiotemporal dynamics of forest aboveground biomass in the ChangZhuTan urban agglomeration using a time series of Landsat images and meteorological data from 2010 to 2020. *Sci. Total. Environ.* 944, 173940. 10.1016/j.scitotenv.2024.173940.

Lu, D., Chen, Q., Wang, G., Liu, L., Li, G. & Moran, E., 2016. A survey of remote sensing-based aboveground biomass estimation methods in forest ecosystems. *Int. J. Digit. Earth* 9(1), 63-105. 10.1080/17538947.2014.990526.

Lu Zhang, X. W., Bing Sun, Tropical natural forest classification using time-series Sentinel-1 and Landsat-8 images in Hainan island. *IGARSS 2019 - 2019 IEEE International Geoscience and Remote Sensing Symposium*. Yokohama, Japan. 6732–6735.

Macave, O. A., Ribeiro, N. S., Ribeiro, A. I., Chaúque, A., Bandeira, R., Branquinho, C. & Washington-Allen, R., 2022. Modelling Aboveground Biomass of Miombo Woodlands in Niassa Special Reserve, Northern Mozambique. *For.* 13(2), 311. 10.3390/f13020311.

Makhado, R. A., Mapaure, I., Potgieter, M. J., Luus-Powell, W. J. & Saidi, A. T., 2014. Factors influencing the adaptation and distribution of Colophospermum mopane in southern Africa's mopane savannas - A review. *Bothalia (Online)* 44(1), 1-9. 10.4102/abc.v44i1.152.

Malhi, R. K. M., Anand, A., Srivastava, P. K., Chaudhary, S. K., Pandey, M. K., Behera, M. D., Kumar, A., Singh, P. & Sandhya Kiran, G., 2021. Synergistic evaluation of Sentinel 1 and 2 for biomass estimation in a tropical forest of India. *Adv. Sp. Res.* 10.1016/j.asr.2021.03.035.

Mareya, H. T., Tagwireyi, P., Ndaimani, H., Gara, T. W. & Gwenzi, D., 2018. Estimating Tree Crown Area and Aboveground Biomass in Miombo Woodlands from High-Resolution RGB-Only Imagery. *IEEE J. Sel. Top. Appl. Earth Obs. Remote Sens.* 11(3), 868-875. 10.1109/JSTARS.2018.2799386.

Mayes, M., Mustard, J., Melillo, J., Neill, C. & Nyadzi, G., 2016. Going beyond the green: senesced vegetation material predicts basal area and biomass in remote sensing of tree cover conditions in an African tropical dry forest (miombo woodland) landscape. *Environ. Res. Lett.* 12(8), 85004. 10.1088/1748-9326/aa7242.

Mcnicol, I. M., Ryan, C. M. & Mitchard, E. T. A., 2018a. Carbon losses from deforestation and widespread degradation offset by extensive growth in African woodlands. *Nat. Commun.* 9(1), 3045-11. 10.1038/s41467-018-05386-z.

Mcnicol, I. M., Ryan, C. M. & Mitchard, E. T. A., 2018b. Carbon losses from deforestation and widespread degradation offset by extensive growth in African woodlands. *Nat. Commun.* 9(1), 3045-3045. 10.1038/s41467-018-05386-z.

Mitchard, E. T. A., Meir, P., Ryan, C. M., Woollen, E. S., Williams, M., Goodman, L. E., Mucavele, J. A., Watts, P., Woodhouse, I. H. & Saatchi, S. S., 2013a. A novel application of satellite radar data: measuring carbon sequestration and detecting degradation in a community forestry project in Mozambique. *Plant Ecol. Divers.* 6(1), 159-170. 10.1080/17550874.2012.695814.

Mitchard, E. T. A., Saatchi, S. S., Baccini, A., Asner, G. P., Goetz, S. J., Harris, N. L. & Brown, S., 2013b. Uncertainty in the spatial distribution of tropical forest biomass: a comparison of pan-tropical maps. *Carbon Balanc. Manag.* 8(1), 10-10. 10.1186/1750-0680-8-10.

Mitchard, E. T. A., Saatchi, S. S., Woodhouse, I. H., Nangendo, G., Ribeiro, N. S., Williams, M., Ryan, C. M., Lewis, S. L., Feldpausch, T. R. & Meir, P., 2009. Using satellite radar backscatter to predict above-ground woody biomass: A consistent relationship across four different African landscapes. *Geophys. Res. Lett.* 36(23), np-n/a. 10.1029/2009GL040692.

Næsset, E., Ørka, H. O., Solberg, S., Bollandsås, O. M., Hansen, E. H., Mauya, E., Zahabu, E., Malimbwi, R., Chamuya, N., Olsson, H. & Gobakken, T., 2016. Mapping and estimating forest area and aboveground biomass in miombo woodlands in Tanzania using data from airborne laser scanning, TanDEM-X, RapidEye, and global forest maps: A comparison of estimated precision. *Remote Sens. Environ.* 175, 282-300. 10.1016/j.rse.2016.01.006.

Navarro, J. A., Algeet, N., Fernández-Landa, A., Esteban, J., Rodríguez-Noriega, P. & Guillén-Climent, M. L., 2019. Integration of UAV, Sentinel-1, and Sentinel-2 data for mangrove plantation aboveground biomass monitoring in Senegal. *Remote Sens. (Basel, Switzerland)* 11(1), 77. 10.3390/rs11010077.

Nicolau, A. P., Flores-Anderson, A., Griffin, R., Herndon, K. & Meyer, F. J., 2021. Assessing SAR C-band data to effectively distinguish modified land uses in a heavily disturbed Amazon forest. *Int. J. Appl. Earth Obs. Geoinf.* 94, 102214. 10.1016/j.jag.2020.102214.

Pearse, G. D., Watt, M. S., Dash, J. P., Stone, C. & Caccamo, G., 2019. Comparison of models describing forest inventory attributes using standard and voxel-based lidar predictors across a range of pulse densities. *Int. J. Appl. Earth Obs. Geoinf.* 78, 341-351. 10.1016/j.jag.2018.10.008.

Phiri, D., Mwitwa, J., Ng'andwe, P., Kanja, K., Munyaka, J., Chileshe, F., Hamazakaza, P., Kapembwa, S. & Kwenye, J. M., 2023. Agricultural expansion into forest reserves in Zambia: a remote sensing approach. *Geocarto Int.* 38(1). 10.1080/10106049.2023.2213203.

Pirotti, F., 2011. Analysis of full-waveform LiDAR data for forestry applications: A review of investigations and methods. *IFor. (Viterbo)* 4(JUNE), 100-106. 10.3832/ifor0562-004.

Qadeer, A., Shakir, M., Wang, L. & Talha, S. M., 2024. Evaluating machine learning approaches for aboveground biomass prediction in fragmented high-elevated forests using multi-sensor satellite data. *Remote Sens. Appl.* 36, 101291. 10.1016/j.rsase.2024.101291.

Quijas, S., Boit, A., Thonicke, K., Murray-Tortarolo, G., Mwampamba, T., Skutsch, M., Simoes, M., Ascarrunz, N., Peña-Claros, M., Jones, L., Arets, E., Jaramillo, V. J., Lazos, E., Toledo, M., Martorano, L. G., Ferraz, R. & Balvanera, P., 2019. Modelling carbon stock and carbon sequestration ecosystem services for policy design: a comprehensive approach using a dynamic vegetation model. *Ecosyst. People (Abingdon, England)* 15(1), 42-60. 10.1080/26395908.2018.1542413.

Rodriguez-Galiano, V. F., Chica-Olmo, M., Abarca-Hernandez, F., Atkinson, P. M. & Jeganathan, C., 2012. Random Forest classification of Mediterranean land cover using multi-seasonal imagery and multi-seasonal texture. *Remote Sens. Environ.* 121, 93-107. 10.1016/j.rse.2011.12.003.

Ryan, C. M., Pritchard, R., Mcnicol, I., Owen, M., Fisher, J. A. & Lehmann, C., 2016. Ecosystem services from southern African woodlands and their future under global change. *Philos. Trans. R. Soc. Lond. B. Biol. Sci.* 371(1703), 20150312. 10.1098/rstb.2015.0312.

Saatchi, S. S., Harris, N. L., Brown, S., Lefsky, M., Mitchard, E. T. A., Salas, W., Zutta, B. R., Buermann, W., Lewis, S. L., Hagen, S., Petrova, S., White, L., Silman, M. & Morel, A., 2011. Benchmark map of forest carbon stocks in tropical regions across three continents. *Proc. Natl. Acad. Sci. U S A* 108(24), 9899-9904. 10.1073/pnas.1019576108.

Salis, S. M., Assis, M. A., Mattos, P. P. & Pião, A. C. S., 2006. Estimating the aboveground biomass and wood volume of savanna woodlands in Brazil's Pantanal wetlands based on allometric correlations. *For. Ecol. Manag.* 228(1), 61-68. 10.1016/j.foreco.2006.02.025.

Shakacite, O., Chungu, D., Ng'andwe, P., Siampale, A. M., Chendauka, B., Vesa, L. & Roberts, W. J.,2016. Integrated Land Use Assessment phase II – report for Zambia. Lusaka, Zambia: Government Printers (The Food and Agriculture Organizationof the United Nations and the Forestry Department, Ministry ofLands and Natural Resources).

Shamaoma, H., Chirwa, P. W., Ramoelo, A., Hudak, A. T. & Syampungani, S., 2022. The Application of UASs in Forest Management and Monitoring: Challenges and Opportunities for Use in the Miombo Woodland. *For.* 13(11), 1812. 10.3390/f13111812.

Syampungani, S., Chirwa, P. W., Akinnifesi, F. K., Sileshi, G. & Ajayi, O. C., 2009. The miombo woodlands at the cross roads: Potential threats, sustainable livelihoods, policy gaps and challenges. *Nat. Resour. Forum* 33(2), 150-159. 10.1111/j.1477-8947.2009.01218.x.

Tanase, M. A., Mihai, M. C., Miguel, S., Cantero, A., Tijerin, J., Ruiz-Benito, P., Domingo, D., Garcia-Martin, A., Aponte, C. & Lamelas, M. T., 2024. Long-term annual estimation of forest above ground biomass, canopy cover, and height from airborne and spaceborne sensors synergies in the Iberian Peninsula. *Environ. Res.* 259, 119432. 10.1016/j.envres.2024.119432.

Tassi, A., Gigante, D., Modica, G., Di Martino, L. & Vizzari, M., 2021. Pixel-vs. Object-based landsat 8 data classification in google earth engine using random forest: The case study of maiella national park. *Remote Sens. (Basel, Switzerland)* 13(12), 2299. 10.3390/rs13122299.

Urbazaev, M., Thiel, C., Mathieu, R., Naidoo, L., Levick, S. R., Smit, I. P. J., Asner, G. P. & Schmullius, C., 2015. Assessment of the mapping of fractional woody cover in southern African savannas using multi-temporal and polarimetric ALOS PALSAR L-band images. *Remote Sens. Environ.* 166, 138-153. 10.1016/j.rse.2015.06.013.

Van Pham, M., Pham, T. M., Viet Du, Q. V., Bui, Q.-T., Van Tran, A., Pham, H. M. & Nguyen, T. N., 2019. Integrating Sentinel-1A SAR data and GIS to estimate aboveground biomass and carbon accumulation for tropical forest types in Thuan Chau district, Vietnam. *Remote Sens. Appl.* 14, 148-157. 10.1016/j.rsase.2019.03.003.

Vizzari, M., 2022. PlanetScope, Sentinel-2, and Sentinel-1 Data Integration for Object-Based Land Cover Classification in Google Earth Engine. *Remote Sens. (Basel, Switzerland)* 14(11), 2628. 10.3390/rs14112628.

Wulder, M. A., White, J. C., Nelson, R. F., Næsset, E., Ørka, H. O., Coops, N. C., Hilker, T., Bater, C. W. & Gobakken, T., 2012. Lidar sampling for large-area forest characterization: A review. *Remote Sens. Environ.* 121**,** 196-209. 10.1016/j.rse.2012.02.001.

Zhao, P., Lu, D., Wang, G., Wu, C., Huang, Y. & Yu, S., 2016. Examining spectral reflectance saturation in landsat imagery and corresponding solutions to improve forest aboveground biomass estimation. *Remote Sens. (Basel, Switzerland)* 8(6)**,** 469-469. 10.3390/rs8060469.

Zhu, X. & Liu, D., 2015. Improving forest aboveground biomass estimation using seasonal Landsat NDVI time-series. *ISPRS J. Photogramm. Remote Sens.* 102**,** 222-231. 10.1016/j.isprsjprs.2014.08.014.

Zimbres, B., Rodríguez-Veiga, P., Shimbo, J. Z., Da Conceição Bispo, P., Balzter, H., Bustamante, M., Roitman, I., Haidar, R., Miranda, S., Gomes, L., Alvim Carvalho, F., Lenza, E., Maracahipes-Santos, L., Abadia, A. C., Do Prado Júnior, J. A., Mendonça Machado, E. L., Dias Gonzaga, A. P., De Castro Nunes Santos Terra, M., De Mello, J. M., Soares Scolforo, J. R., Rodrigues Pinto, J. R. & Alencar, A., 2021. Mapping the stock and spatial distribution of aboveground woody biomass in the native vegetation of the Brazilian Cerrado biome. *For. Ecol. Manag.* 499**,** 119615. 10.1016/j.foreco.2021.119615.